Proceedings of the
47th IEEE Conference on Decision and Control
Cancun, Mexico, Dec. 9-11, 2008

Control of Distributed Parameter Systems Subject to Convex Constraints: Applications to Irrigation Systems and Hypersonic Vehicles

Oguzhan Cifdaloz, Armando A. Rodriguez and J. Marty Anderies

Abstract— **This paper addresses designing finite dimensional linear time invariant (LTI) controllers for infinite dimensional LTI plants subject to $\mathcal{H}^\infty$ mixed-sensitivity performance objectives and convex constraints. Specifically, we focus on designing control systems for two classes of systems which are generally described by hyperbolic partial differential equations: (1) Irrigation systems and (2) Hypersonic Vehicles with flexible dynamics. The distributed parameter plant is first approximated by a finite dimensional approximant. The Youla parameterization is then used to parameterize the set of all stabilizing LTI controllers and a weighted mixed-sensitivity $\mathcal{H}^\infty$ optimization is formulated. After transforming the infinite dimensional problem to a finite-dimensional optimization problem, convex is optimization is used to obtain the solution. Subgradient concepts are used to directly accommodate time-domain specifications. Illustrative examples for irrigation systems and hypersonic vehicles are provided.**

I. INTRODUCTION AND MOTIVATION

A. Irrigation Systems

Irrigation is an increasingly important issue worldwide. Irrigation systems may be required for several key reasons in crop production. These may include: delivering water to an arid area, draining water from a wet area, providing supplements, protecting against frost and weed growth. Water management becomes particularly important in order to properly (and fairly) address water right conflicts. Most irrigation canals are operated using gates placed upstream and/or downstream. We use the classic Saint Venant equations (nonlinear hyperbolic PDEs) to describe gravity-based laminar fluid flow in canals and rivers. In this paper, we linearize these equations to obtain a model suitable for control design. The model is used to design near-optimal weighted $\mathcal{H}^\infty$ controllers subject to (convex) constraints.

B. Hypersonic Vehicles

With the historic 2004 scramjet-powered Mach 7 and 10 flights of the X-43A hypersonics research has seen a resurgence. This is attributable to the fact that air-breathing hypersonic propulsion is viewed as the next critical step toward achieving (1) reliable affordable access to space, (2) global reach vehicles. Both of these applications have commercial as well as military implications. While rocket-based (combined cycle) propulsion systems are needed to reach orbital speeds, they are much more expensive to operate because they must carry oxygen. This is particularly costly when travelling at lower altitudes through the troposphere. Current rocket-based systems also do not exhibit the desired levels of reliability and flexibility (e.g. with a landing option). For this reason, much emphasis has been placed on two-stage-to-orbit (TSTO) designs which involve a turbo-ram-scramjet combined cycle first stage and a rocket-scramjet second stage. Hypersonic vehicles are characterized by significant aero-thermo-elastic-propulsion interactions and uncertainty. Such vehicles are generally characterized by unstable non-minimum phase dynamics as well as uncertain (hyperbolic) flexible dynamics. A nonlinear model for the longitudinal dynamics of a scramjet-powered hypersonic vehicle has been used as the basis for our analysis and design.

C. Control Design Methodology

In this work, the distributed parameter plant is first approximated by a finite dimensional approximant. For unstable plants, the coprime factors are approximated by their finite dimensional approximants. The Youla parameterization is then used to parameterize the set of all stabilizing LTI controllers and formulate a weighted mixed-sensitivity $\mathcal{H}^\infty$ optimization that is convex in the Youla $Q-$Parameter. A finite-dimensional (real rational) stable basis is used to approximate the $Q-$parameter. By so doing, the associated infinite-dimensional optimization problem is transformed to a finite-dimensional optimization problem involving a search over a finite-dimensional parameter space. In addition to solving weighted mixed-sensitivity $\mathcal{H}^\infty$ control system design problems, subgradient concepts are used to directly accommodate time-domain specifications (e.g. peak value of control action, overshoot) in the design process. As such, a systematic design methodology is provided for a large class of distributed parameter plant control system design problems. Convergence results are presented. Illustrative examples for irrigation systems and hypersonic vehicles are provided. In short, the approach taken permits a designer to address control system design problems for which no direct method exists. Detailed description of the design methodology used can be found in [1], [2], [3].

This paper is organized as follows: Section II describes the open channel system model, Section III describes the hypersonic vehicle model, Section IV describes the control design methodology used, Section V presents the control designs, Section VI presents a summary and directions for future research.

O. Cifdaloz is a postdoctoral research associate at Department of Electrical Engineering, Ira A. Fulton School of Engineering, Arizona State University, Tempe, AZ 85287. ogu@asu.edu

A. A. Rodriguez is with the Intelligent Embedded Systems Laboratory (IeSL), Department of Electrical Engineering, Ira A. Fulton School of Engineering, Arizona State University, Tempe, AZ 85287. aar@asu.edu

J. M. Anderies is with the Center for the Study of Institutional Diversity School of Human Evolution and Social Change, Arizona State University, Tempe, AZ 85287. anderies@asu.edu

978-1-4244-3124-3/08/$25.00 ©2008 IEEE

II. IRRIGATION SYSTEM MODEL

The Saint Venant equations (named after Adhémar Jean Claude Barré de Saint-Venant) are a set of hyperbolic partial differential equations that describe the flow below a pressure surface in a fluid. The following form of the St. Venant equations is used to describe open-channel flow:

$$\frac{\partial A}{\partial t} + \frac{\partial Q}{\partial x} = 0 \tag{1}$$

$$\frac{\partial Q}{\partial t} + \frac{\partial Q^2/A}{\partial x} + gA\frac{\partial Y}{\partial x} + gA(S_f - S_b) = 0 \tag{2}$$

$$Q(0,t) = u_1(t), \qquad Q(L,t) = u_2(t) \tag{3}$$

$$Q(x,0) = Q_o, \qquad Y(x,0) = Y_o \tag{4}$$

Equation 1 is called the continuity equation, Equation 2 is called the momentum equation, and Equations 3 and 4 define the boundary and initial conditions, respectively. Variables and parameters used in Equations 1–4 are given in Table I and illustrated in Fig.1.

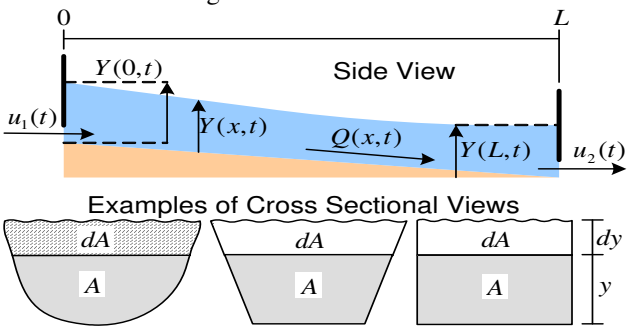

Fig. 1. Canal Structure Schematic

TABLE I

St. Venant Equations: Descriptions of Variables and Parameters

Symbol	Description	Unit
$A(x,t)$	wetted area	m^2
$Q(x,t)$	total discharge across section $A(x,t)$	m^3/s
$Y(x,t)$	water depth	m
$S_f(x,t)$	friction slope	–
$S_b(x,t)$	bed slope (assumed constant)	–
x	distance in the direction of flow	m
t	time	s
g	acceleration due to gravity	m/s^2
L	length of channel	m
$u_i(t)$	control flow rates	m^3/s

The friction slope, S_f, is modelled using the Manning–Strickler formula [4]:

$$S_f = \frac{Q^2 n^2}{A^2 R^{4/3}} \tag{5}$$

where n represents Manning's resistance coefficient $(s/m^{1/3})$, R represents hydraulic radius $\stackrel{\text{def}}{=} A/P$ (m), and P represents hydraulic perimeter (m).

Assuming a *prismatic channel*, which allowes $A_o = T_o Y_o$ where T_o is the width of channel at surface level, and linearizing 1–2 yields [5]

$$T_o\,\frac{\partial y}{\partial t} + \frac{\partial q}{\partial x} = 0 \tag{6}$$

$$\frac{\partial q}{\partial t} + 2\,V_o\,\frac{\partial q}{\partial x} + (C_o^2 - V_o^2)\,T_o\,\frac{\partial y}{\partial x} - \beta_o\,q - \gamma_o\,y = 0 \tag{7}$$

$q(x,t)$ and $y(x,t)$ represent "small" variations from $Q_o(x,t)$ and $Y_o(x,t)$, respectively. In Equations 6-7, $F_o \stackrel{\text{def}}{=} V_o/C_o$ is the Froude number, $C_o \stackrel{\text{def}}{=} \sqrt{g\frac{A_o}{T_o}}$ (m/s) is the celerity, $V_o \stackrel{\text{def}}{=} \frac{Q_o}{A_o}$ (m/s) is the mean fluid velocity . β_o and γ_o are given by [5]:

$$\beta_o = -\frac{2g}{V_o}\left(S_b - \frac{dY_o}{dx}\right) \tag{8}$$

$$\gamma_o = V_o^2\frac{dT_o}{dx} + gT_o\left\{(1+\kappa)S_b - \left[1+\kappa-(\kappa-2)F_o^2\right]\frac{dY_o}{dx}\right\} \tag{9}$$

where

$$\kappa = \frac{7}{3} - \frac{4}{3}\frac{A_o}{T_o P_o}\frac{\partial P_o}{\partial Y}. \tag{10}$$

It is assumed that $F_o < 1$ (laminar flow).

By taking the Laplace Transform of Equations 6-7 and solving for $q(x,s)$ and $y(x,s)$ we obtain the following infinite dimensional transfer functions:

$$q(x,s) = \frac{e^{\lambda_2 L}e^{\lambda_1 x} - e^{\lambda_1 L}e^{\lambda_2 x}}{e^{\lambda_2 L} - e^{\lambda_1 L}}u_1 + \frac{e^{\lambda_2 x} - e^{\lambda_1 x}}{e^{\lambda_2 L} - e^{\lambda_1 L}}u_2 \tag{11}$$

$$y(x,s) = -\frac{1}{T_o s}\frac{\lambda_1 e^{\lambda_2 L}e^{\lambda_1 x} - \lambda_2 e^{\lambda_1 L}e^{\lambda_2 x}}{e^{\lambda_2 L} - e^{\lambda_1 L}}u_1 - \frac{1}{T_o s}\frac{\lambda_2 e^{\lambda_2 x} - \lambda_1 e^{\lambda_1 x}}{e^{\lambda_2 L} - e^{\lambda_1 L}}u_2 \tag{12}$$

where

$$\lambda_{1,2}(s) = \frac{2V_oT_os + \gamma_o}{2(C_o^2 - V_o^2)T_o} \pm \frac{\sqrt{(2V_oT_os + \gamma_o)^2 + 4s(C_o^2 - V_o^2)T_o^2(s - \beta_o)}}{2(C_o^2 - V_o^2)T_o} \tag{13}$$

Equation 12 can be visualized as shown in Fig. 2.

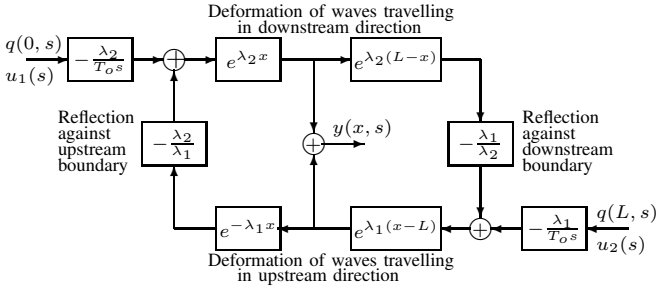

Fig. 2. Block diagram of open channel flow in a reach [6]

Equations 12 and 13 leads to the 2-input 1-output Saint-Venant transfer function matrix [7]:

$$y(x,s) = \left[\frac{\lambda_2 e^{\lambda_1 L}e^{\lambda_2 x} - \lambda_1 e^{\lambda_2 L}e^{\lambda_1 x}}{T_o s(e^{\lambda_2 L} - e^{\lambda_1 L})} \quad \frac{\lambda_1 e^{\lambda_1 x} - \lambda_2 e^{\lambda_2 x}}{T_o s(e^{\lambda_2 L} - e^{\lambda_1 L})}\right]\begin{bmatrix}u_1\\ u_2\end{bmatrix} \tag{14}$$

A low frequency approximation of this transfer function can be given as [7]:

$$y(x,s) = \begin{bmatrix} \frac{e^{-s\hat{\tau}_d(x)}}{\hat{A}_d(x)(s+\alpha)} & -\frac{1}{\hat{A}_d(x)(s+\alpha)}\end{bmatrix}\begin{bmatrix}u_1(s)\\ u_2(s)\end{bmatrix} \tag{15}$$

with the equivalent downstream backwater area, $\hat{A}_d(x)$, and the downstream delay, $\hat{\tau}_d(x)$, and a seepage factor, α.

The equivalent downstream backwater area, $\hat{A}_d(x)$, is given by

$$\hat{A}_d(x) \;=\; A_d(L-x)\left(1 + \frac{A_d(x)}{A_u(L-x)}\right) \tag{16}$$

where

$$A_d(x) = \frac{T_o^2(C_o^2 - V_o^2)}{\gamma_o}\left(1 - e^{-\frac{\gamma_o}{T_o(C_o^2-V_o^2)}x}\right), \quad (17)$$

$$A_u(x) = \frac{T_o^2(C_o^2 - V_o^2)}{\gamma_o}\left(e^{\frac{\gamma_o}{T_o(C_o^2-V_o^2)}x} - 1\right). \quad (18)$$

The equivalent downstream delay, $\hat{\tau}_d(x)$, is given by

$$\hat{\tau}_d(x) = \tau_d(x) + \tau_d(L-x) \quad \text{where} \quad \tau_d = \frac{x}{C_o + V_o}. \quad (19)$$

III. HYPERSONIC VEHICLE MODEL

A scramjet (supersonic combustion ramjet) powered hypersonic wave-rider is characterized by significant aero-thermo-elastic-propulsion interactions and uncertainty [8]. Such interactions include viscous shock and boundary layer interactions as well as nonlinear coupling associated with a tightly integrated vehicle and propulsion system. The nonlinear dynamical model [8] captures the vehicle's longitudinal rigid body dynamics, hypersonic aerodynamics, atmospheric effects, structural dynamical coupling, and vehicle-scramjet propulsion coupling effects.

Given the historic 2004 X-43A scramjet powered hypersonic flights at Mach 7 and 10, the scramjet is of particular interest. A scramjet is a variation of a ramjet with the key difference being that the flow in the combustor is supersonic. Like a ramjet, a scramjet essentially consists of a constricted tube through which inlet air is compressed by the high speed of the vehicle, fuel is combusted, and then the exhaust leaves at higher speed than the inlet air.

What makes this application interesting is that the associated aero-thermo-elastic-propulsion interactions are governed by several systems of coupled partial differential equations (PDEs). Navier-Stokes describes the basic fluid and aerodynamics. Oblique shock and Prandtl-Meyer expansion theory are used to simplify pressure computations and make substantive simplifications [9], [10]. The vehicle relies on compression lift provided by the forebody which serves as a compressor for the scramjet. The underbelly of the vehicle aftbody makes up the scramjet. As such, vehicle flexing is critical because it impacts the bow shock angle and air flow into the scramjet inlet. Vehicle flexing is modeled by fore and aft cantilever Euler-Bernoulli beams. The scramjet, which is also governed by the Navier-Stokes equations, is modeled by a simple fixed geometry duct with heat addition. Travel at hypersonic speeds can result in very high temperatures which significantly impact the structural dynamics. Such effects will not be examined here but, in general, are described by PDEs involving conduction, convection, and radiation terms. At sufficiently low densities (large Knudsen numbers), Navier-Stokes breaks down and Boltzmann-based kinetic theory must be used. This too will not be considered here.

The variables to be controlled are speed and flight path angle. The linear model is obtained by trimming the nonlinear model at $V_o = 8M$ and $z_o = 85000\ ft$. States of the model are given as

$$x = [V \ \ \gamma \ \ q \ \ \theta \ \ \eta_1 \ \ \dot{\eta}_1 \ \eta_2 \ \ \dot{\eta}_2 \ \eta_3 \ \ \dot{\eta}_3] \quad (20)$$

where V, γ, q, and θ represent variations in the basic 3-dof rigid body modes, i.e. speed (ft/sec), flight path angle (deg), pitch rate (deg/sec), and pitch angle (deg), respectively. η_i and $\dot{\eta}_i$ $(i = 1, 2, 3)$ represent flexible modes. Control inputs are given as

$$u = [\delta_e \ \ \delta_{FER}] \quad (21)$$

where δ_e and δ_{FER} represent variations in elevator angle (deg) and fuel equivalence ratio.

The plant approximant singular values are shown in Fig. 3 as more modes are included. The first body bending mode is observed to lie near 20 rad/sec. Given the performance objectives, it was deemed that 3 flexible modes would be adequate.

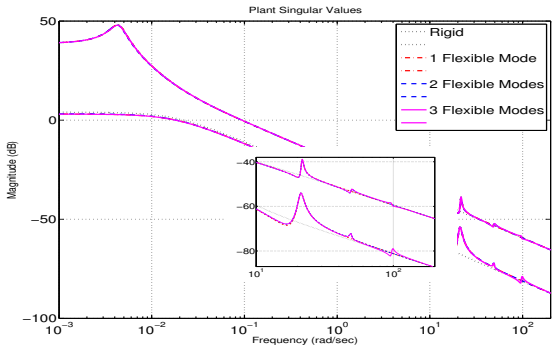

Fig. 3. Plant Singular Values

IV. CONTROL DESIGN METHODOLOGY

In this section, stable plants are used to present the main ideas. It should be noted, however, that all of the ideas and results presented can be extended to unstable plants. This is discussed in [1], [3]. Results for $\mathcal{H}^\infty$ mixed-sensitivity minimization for stable infinite-dimensional plants without constraints are given in [2].

Proposition 4.1: (***Stabilizing Compensators***). Given N_p, $D_p, \tilde{N}_p, \tilde{D}_p, N_k, D_k, \tilde{N}_k, \tilde{D}_k \in \mathcal{H}^\infty$, let

$$P = N_p D_p^{-1} = \tilde{D}_p^{-1}\tilde{N}_p \quad (22)$$

be right and left co-prime factorizations of P, and

$$\begin{bmatrix} \tilde{D}_k & -\tilde{N}_k \\ -\tilde{N}_p & \tilde{D}_p \end{bmatrix}\begin{bmatrix} D_p & N_k \\ N_p & D_k \end{bmatrix} = \begin{bmatrix} I & 0 \\ 0 & I \end{bmatrix} \quad (23)$$

is the corresponding *Bezout* identity. Then, the set of all proper controllers, $S(P) \stackrel{\text{def}}{=} \{K(P,Q) | Q \in \mathcal{H}^\infty\}$ which internally stabilize P is given by:

$$K(P,Q) = (N_k - D_p Q)(D_k - N_p Q)^{-1} \quad (24)$$

$$= (\tilde{D}_k - Q\tilde{N}_p)^{-1}(\tilde{N}_k - Q\tilde{D}_p) \quad (25)$$

Let $P(s) \in \mathcal{H}^\infty$ denote a stable MIMO transfer function matrix for a distributed parameter plant. Also, let $\{P_n(s)\}_{n=1}^\infty \in R\mathcal{H}^\infty$ denote a sequence of stable finite-dimensional approximants for P. In order to present the main ideas, it is useful to define the following performance measure.

Definition 4.1: (***Mixed-Sensitivity***). Suppose W_1, W_2, W_3, $F, G, H \in \mathcal{H}^\infty$, and $K(G,H)$ internally stabilizes F (as well as G). The *mixed-sensitivity* of the pair $(F, K(G,H))$, denoted J_{mix}, is defined as the map $J_{\text{mix}}(\cdot, K(\cdot,\cdot)) : \mathcal{H}^\infty \times$

$\mathcal{H}^\infty \times \mathcal{H}^\infty \to R_+$ where

$$J_{\rm mix}(F, K(G,H)) \stackrel{\rm def}{=} \left\| \begin{bmatrix} W_1 \\ W_2 K(G,H) \\ W_3 F K(G,H) \end{bmatrix} (I - FK(G,H))^{-1} \right\|_{\mathcal{H}^\infty}. \quad (26)$$

Comment 4.1: **(Mixed-Sensitivity).** It should be noted that $K(G,H)$ need not belong to $\mathcal{H}^\infty$. This follows from the fact that not every plant is stabilizable by a stable controller. It should also be noted that in what follows three specific cases will be considered: (1) $F = G = P$ is an infinite-dimensional plant, (2) $F = G = P_n$ is a finite-dimensional approximant for P, (3) $F = P$ and $G = P_n$. In all cases H will represent a stable Q parameter which is generally infinite-dimensional in case (1) and finite-dimensional in cases (2) and (3).

The *optimal performance* for the distributed parameter plant P with respect to the measure $J_{\rm mix}$ is defined as follows:

Definition 4.2: **(Optimal Performance)**

$$\mu_{opt}(\gamma_c) \stackrel{\rm def}{=} \inf_{Q \in \mathcal{H}^\infty} \{\, J_{\rm mix}(P, K(P,Q)) \;\mid\; C(T_{cl}(P, K(P,Q))) < \gamma_c \,\} \quad (27)$$

where $C(T_{cl}(P, K(P,Q)))$ denotes convex constraints on the associated closed loop maps $T_{cl}(P, K(P,Q))$ and $\gamma_c \in [0, \infty]$ denotes a constraint parameter selected by the designer. $\gamma_c = \infty$ corresponds to the unconstrained case.

Since P is infinite-dimensional and $Q \in \mathcal{H}^\infty$, it follows that the controller $K(P,Q) = -Q(I - PQ)^{-1}$ is generally infinite-dimensional.

Figure 4 shows a near-optimal controller K_o for P. In general, determining K_o is difficult. Specific unconstrained cases have been addressed within [11], [12], [13], [14].

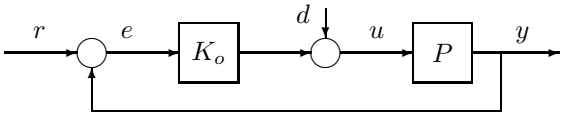

Fig. 4. Near-Optimal Infinite-Dimensional Feedback Loop

The above optimization problem is the central problem being considered. The approach taken here requires that P be (suitably) approximated by a finite-dimensional system P_n. This motivates the following finite-dimensional optimization.

Definition 4.3: **(Expected Performance)**

$$\mu_n(\gamma_c) \stackrel{\rm def}{=} \inf_{Q \in R\mathcal{H}^\infty} \{\, J_{\rm mix}(P_n, K(P_n,Q)) \;\mid\; C(T_{cl}(P_n, K(P_n,Q))) < \gamma_c \,\} \quad (28)$$

where $C(T_{cl}(P_n, K(P_n,Q)))$ denotes convex constraints on the associated closed loop maps $T_{cl}(P_n, K(P_n,Q))$.

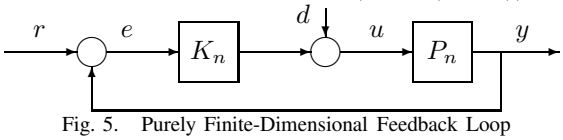

Fig. 5. Purely Finite-Dimensional Feedback Loop

Since $P_n \in R\mathcal{H}^\infty$ is finite-dimensional, it follows that $K(P_n, Q) = -Q(I - P_n Q)^{-1}$ is finite-dimensional when $Q \in R\mathcal{H}^\infty$. While well known (Riccati, LMI) methods exist for the unconstrained case [15], [16], mainly numerical approaches exist for the constrained case [17], [18]. Here, $\mu_n(\gamma_c)$ will be referred to as the *expected performance* since the numbers $\mu_n(\gamma_c)$ provide guidance during design.

Let Q_n denote any optimal or near-optimal solution to the problem in Definition 4.3. By the parameterization given in Proposition 4.1, it follows that Q_n generates an internally stabilizing compensator K_n for P_n (see Figure 5):

$$K_n \stackrel{\rm def}{=} K(P_n, Q_n) \stackrel{\rm def}{=} -Q_n(I - P_n Q_n)^{-1}. \quad (29)$$

Because, in general, K_n may not be near-optimal with respect to $\mu_{opt}(\gamma_c)$ as defined in Definition 4.2, and in fact not even stabilizing for P, care must be taken. These issues motivate the following question which underscores the approach taken and the purpose of this work:

Under what conditions on the performance measure $J_{\rm mix}$ and the approximants $\{P_n(s)\}_{n=1}^\infty$, can one ensure that Q_n generates a stabilizing compensator K_n which delivers near-optimal performance for the distributed plant P?

This question leads one to naturally consider the feedback system obtained by substituting the finite-dimensional compensator K_n into a closed loop system with the distributed plant P (see Figure 6). Assuming that internal stability can be shown [19], this then motivates the following "natural" definition for the *actual performance*.

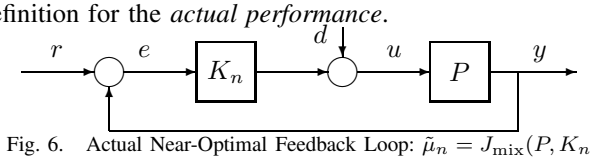

Fig. 6. Actual Near-Optimal Feedback Loop: $\tilde{\mu}_n = J_{\rm mix}(P, K_n)$

Definition 4.4: **(Actual Performance)**

$$\tilde{\mu}_n(\gamma_c) \stackrel{\rm def}{=} J_{\rm mix}(P, K_n) \quad (30)$$

The main goal of the paper is to design a finite-dimensional controller K_n, based on the finite-dimensional approximant P_n, that internally stabilizes and delivers near-optimal performance for the infinite-dimensional plant P. This motivates the so-called *Approximate/Design Problem*.

Problem 4.1: **(Approximate/Design).** Find conditions on the performance measure $J_{\rm mix}$ and the approximants $\{P_n\}_{n=1}^\infty$ such that

$$\lim_{n \to \infty} \tilde{\mu}_n(\gamma_c) = \mu_{opt}(\gamma_c). \quad (31)$$

In practice, one would like to be able to compute $\mu_{opt}(\gamma_c)$ using finite-dimensional algorithms. With the ultimate intention of providing such algorithms, the following *"Purely" Finite-Dimensional Weighted $\mathcal{H}^\infty$ Mixed-Sensitivity Problem* is considered.

Problem 4.2: **(Purely Finite-Dimensional).** Find conditions on the performance measure $J_{\rm mix}$ and the approximants $\{P_n\}_{n=1}^\infty$ such that

$$\lim_{n \to \infty} \mu_n(\gamma_c) = \mu_{opt}(\gamma_c). \quad (32)$$

Solutions to the above constrained problems (Problems 4.1-4.2) will be presented below. A proof will be given for the specific constraint:

$$C(T_{cl}(P, K(P,Q))) = \left\| \begin{bmatrix} W_{1c}(I - PQ) \\ W_{2c} Q \\ W_{3c} PQ \end{bmatrix} \right\|_{\mathcal{H}^\infty} < \gamma_c. \quad (33)$$

Solutions to the *Approximate/Design Problem* and the *Purely Finite-Dimensional Problem* are provided in [1], [2], [3].

V. CONTROL DESIGNS

In this section an irrigation control system design and a hypersonic vehicle control systems design is presented.

A. Irrigation System Control Design

The description of the irrigation system is given in Section II. In this example, $g = 9.8$, $S_b = 0.001$, $L = 1000$m, $T_o = 2$m, $Y_o = 1$m, $V_o = 1$m/s, $Q_o = 2$ m^3/s, $\alpha = 0.001$s^{-1}, and the point at which the water level is controlled is $x = 750$m. Given these parameters, the approximate St.Venant transfer function is

$$P = \frac{1}{596.75}\begin{bmatrix} \dfrac{e^{-242s}}{s+0.001} & \dfrac{1}{s+0.001} \end{bmatrix}. \quad (34)$$

The finite dimensional approximants P_n used are obtained by approximating the delay by its $[n, n]$ Padé approximations. These approximants satisfy $\lim_{n \to \infty} \|P_n - P\|_{\mathcal{H}^\infty} = 0$ as required.

The mixed-sensitivity problem is defined by the weighting functions

$$W_1 = \frac{0.1s + 0.005}{s + 5 \times 10^{-6}} \quad \text{and} \quad W_2 = \frac{s + 10}{0.001s + 100} I_2. \quad (35)$$

To approximate the Q-parameter, we use the basis

$$q_k = \left(\frac{s-5}{s+5}\right)^{k-1} \quad \text{with} \quad N = 3 \quad \text{terms}. \quad (36)$$

Suppose that we would like to raise the water level at $x = 750$m for 0.5m.

Design 1: Unconstrained Case. Resulting μ_n and $\tilde{\mu}_n$ values for the unconstrained case converge to 0.5646 after $n = 7$.

Closed Loop Time Responses. The associated closed loop output and control responses given in Fig. 7. Fig. 7 shows

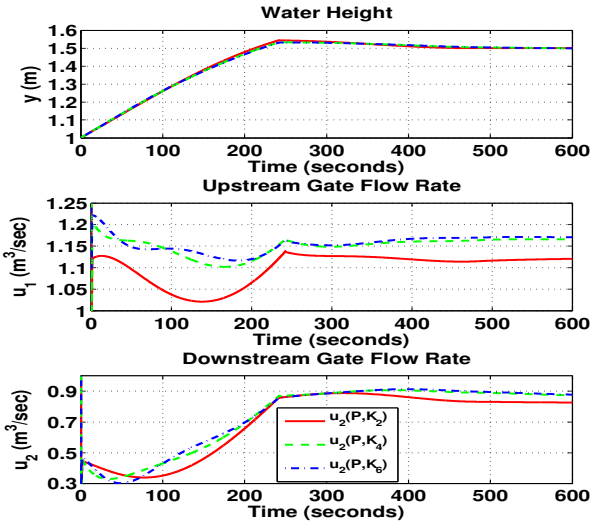

Fig. 7. Irrigation System: Unconstrained Time Responses

that the water level is increased from 1.0m to 1.5 meters in about 5 minutes. In order to achieve this, downstream gate flow is reduced to $0.3m^3/s$, and upstream gate flow rate is reduced to about $1.0m^3/s$ from their nominal values, $Q_o = 2m^3/s$.

Design 2: Constrained Case. Under the constraints that the water discharge at the gates satisfy $u_1(t) \leq Q_o = 2$m^3/sec and $0.63 \leq u_2(t) \leq Q_o = 2$m^3/sec, resulting μ_n and $\tilde{\mu}_n$ values converge to 0.8618 after $n = 3$.

Closed Loop Time Responses. The associated closed loop output and control responses given in Fig. 8.

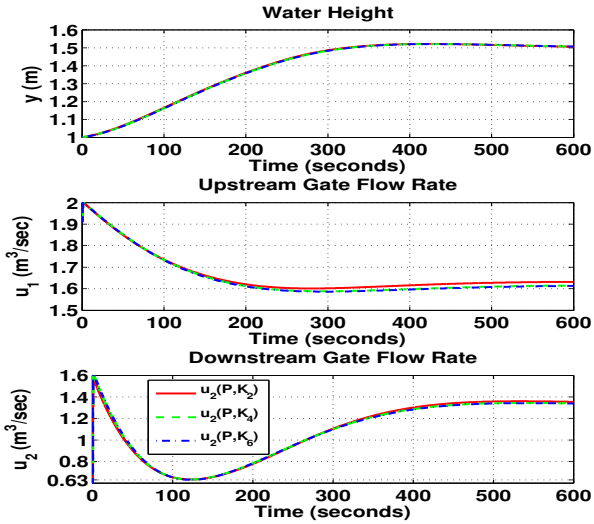

Fig. 8. Irrigation System: Constrained Time Responses

Fig. 8 shows that the water level is increased from 1.0m to 1.5 meters in about 5 minutes. In order to achieve this, downstream gate flow is reduced to $0.63m^3/s$ as required, and upstream gate flow rate is reduced to about $1.6m^3/s$ from their nominal values, $Q_o = 2m^3/s$.

B. Hypersonic Vehicle Control Design

The description of the plant is given in Section III. At the given flight condition, the equilibrium values for speed, elevator angle, and the fuel equivalence ratio are $V_o = 7.8464\ kft/s$, $\delta_{e_o} = 9.5842\ deg$, and $\delta_{FER_o} = 0.4567$, respectively. These values are included in the analysis.

The mixed-sensitivity problem is defined by the weighting functions

$$W_1 = \begin{bmatrix} \frac{0.1s+0.02}{s+2\times10^{-5}} & 0 \\ 0 & \frac{0.1s+0.1}{s+10^{-4}} \end{bmatrix}, W_2 = \begin{bmatrix} \frac{s+100}{10^{-3}s+10^4} & 0 \\ 0 & \frac{s+1000}{10^{-3}s+10^4} \end{bmatrix},$$

$$\text{and} \quad W_3 = \begin{bmatrix} \frac{s+0.04}{10^{-3}s+0.4} & 0 \\ 0 & \frac{s+0.2}{10^{-3}s+2} \end{bmatrix}. \quad (37)$$

To approximate the Q-parameter, we use the basis

$$q_k = \left(\frac{s-10}{s+10}\right)^{k-1} \quad \text{with} \quad N = 4 \quad \text{terms}. \quad (38)$$

Design 1: Unconstrained Case. Resulting μ_n values for the unconstrained $\mathcal{H}^\infty$ problem converge to 11.72.

Closed Loop Time Responses. The associated closed loop output and control responses given in Figs. 9 and 10. Fig. 9

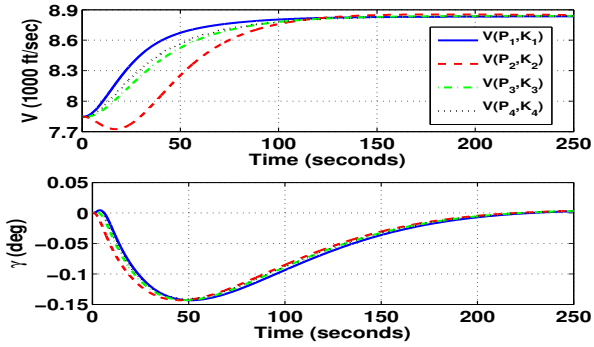

Fig. 9. Hypersonic Vehicle: Unconstrained Output Time Responses

shows that in the unconstrained case settling time for speed is about 120 seconds and there is very small variation in the flight path angle response. Corresponding elevator angle and fuel equivalency ratio responses are given in Fig. 10.

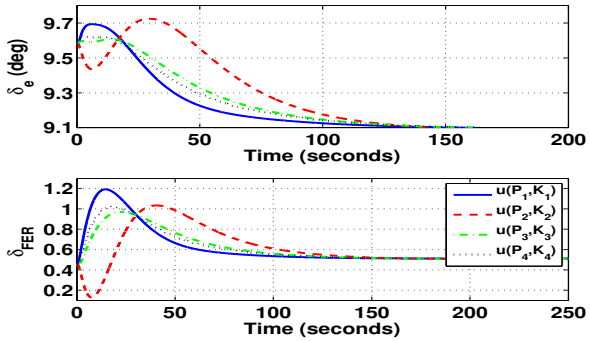

Fig. 10. Hypersonic Vehicle: Unconstrained Control Time Responses

Design 2: Constrained Case. Suppose we would like to limit the fuel equivalence ratio signal such that $\delta_{FER} \leq 0.9$. Imposing this time domain constraint results in μ_n values for the $\mathcal{H}^\infty$ problem to converge to 11.73.

Closed Loop Time Responses. The associated closed loop output and control responses given in Figs. 11 and 12. Fig. 11

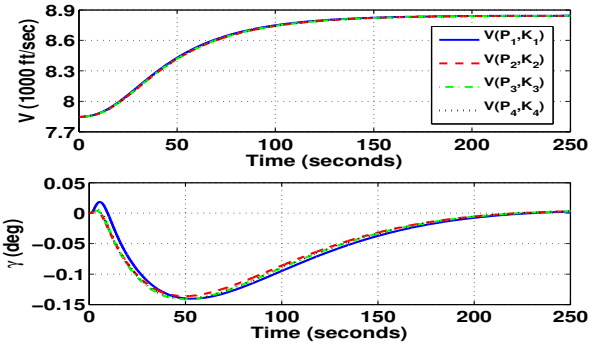

Fig. 11. Hypersonic Vehicle: Constrained Output Time Responses

shows that in the constrained case settling time for speed is about 130 seconds and there is very small variation in the flight path angle response, as in the unconstrained case. However, $\delta_{FER} \leq 0.9$ is satisfied as more flexible modes are included (Fig. 12).

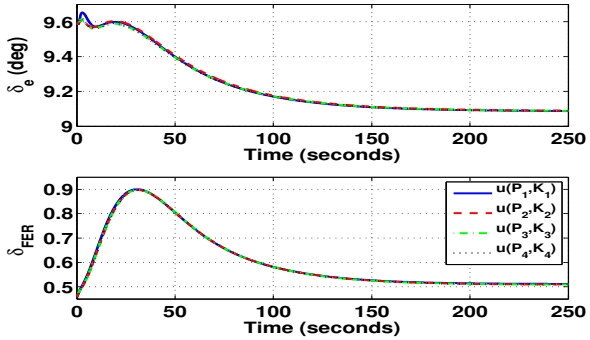

Fig. 12. Hypersonic Vehicle: Constrained Control Time Responses

VI. SUMMARY AND FUTURE DIRECTIONS

This paper has shown how convex optimization may be used to determine $\mathcal{H}^\infty$ near-optimal finite-dimensional controllers for distributed parameter plants subject to convex constraints. Two illustrative examples have been given. Future work will examine other convex constraints and convergence issues [20], [21], [22], examine the impact of temperature effects on aero-elastic properties and control for the hypersonic vehicle, more complicated canal structures and canal networks for the open channel flow.

References

[1] O. Cifdaloz, "$\mathcal{H}^\infty$ mixed-sensitivity optimization for infinite dimensional plants subject to convex constraints," Ph.D. dissertation, Arizona State University, 2007.

[2] A. A. Rodriguez, "Weighted $\mathcal{H}^\infty$ mixed-sensitivity minimization for stable MIMO distributed parameter plants," *IMA J. Mathematical Control and Information*, pp. 219–233, 1995.

[3] A. A. Rodriguez, O. Cifdaloz, R. McCullen, and J. Dickeson, "$\mathcal{H}^\infty$ mixed-sensitivity optimization for distributed parameter plants subject to convex constraints," in *Proc. Conf. Decision and Control*, New Orleans, LA, December 12–14 2007, pp. 866–871.

[4] D. B. Simons and F. Senturk, *Sediment Transport Technology*. Fort Collins, CO: Water Resources Publications, 1992.

[5] X. Litrico and V. Fromion, "Frequency modeling of open-channel flow," *J. Hydraulic Engineering*, vol. 130, no. 8, pp. 806–815, 2004.

[6] J. Schuurmans, O. H. Bosgra, and R. Brouwer, "Open-channel flow model approximation for controller design," *J. Applied Mathematical Modelling*, vol. 19, no. 9, pp. 525–530, 1995.

[7] X. Litrico and V. Fromion, "Analytical approximation of open-channel flow for controller design," *J. Applied Mathematical Modelling*, vol. 28, no. 7, pp. 677–695, 2004.

[8] M. A. Bolender and D. B. Doman, "A nonlinear longitudinal dynamical model of an air-breathing hypersonic vehicle," in *Proc. AIAA Guidance, Navigation, and Control Conf.*, 2005.

[9] A. H. Shapiro, *The Dynamics and Thermodynamics of Compressible Fluid Flow*. Ronald Press, 1953.

[10] J. G. Jones, "Shock-expansion theory and simple wave perturbation," *Journal of Fluid Mechanics Digital Archive*, vol. 17, no. 506–512, 1963.

[11] D. S. Flamm, "Control of delay systems for minimax sensitivity," Ph.D. dissertation, Massachusetts Institute of Technology, 1986.

[12] K. Lenz, H. Ozbay, A. Tannenbaum, J. Turi, and B. Morton, "Robust control design for a flexible beam using a distributed parameter $\mathcal{H}^\infty$ method," in *Proc. Conf. on Decision and Control*, 1989, pp. 2673 – 2678.

[13] H. Özbay and A. Tannenbaum, "On approximately optimal $\mathcal{H}^\infty$ controllers for distributed systems," in *Proc. Conf. on Decision and Control*, vol. 2, 1989, pp. 1454–1459.

[14] K. Kashima, H. Ozbay, and Y. Yamamoto, "A Hamiltonian-based—solution to the mixed sensitivity optimization problem for stable pseudorational plants," *Systems & Control Letters*, vol. 54, no. 11, pp. 1063–1068, 2005.

[15] K. Zhou and J. C. Doyle, *Essentials of Robust Control*. Upper Saddle River, NJ: Prentice Hall, 1998.

[16] K. Zhou, J. C. Doyle, and K. Glover, *Robust and Optimal Control*. Prentice Hall, 1996.

[17] S. P. Boyd and C. H. Barratt, *Linear Controller Design: Limits of Performance*. Englewood Cliffs, NJ: Prentice Hall, 1991.

[18] M. Sznaier, T. Amishima, and T. Inanc, "$\mathcal{H}^2$ control with time-domain constraints: Theory and an application," *IEEE Trans. on Automatic Control*, vol. 48, no. 9, pp. 355–368, 2003.

[19] C. A. Desoer and M. Vidyasagar, *Feedback Systems: Input-Output Properties*. Academic Press, 1975.

[20] A. Quadrat, "On a generalization of the Youla-Kučera parametrization. part i: The fractional ideal approach to SISO systems," *Systems & Control Letters*, vol. 50, pp. 135–148, 2003.

[21] A. Howell and J. K. Hedrick, "Nonlinear observer design via convex optimization," in *Proc. American Control Conf.*, vol. 3, 2002, pp. 2088–2093.

[22] A. A. Rodriguez, "Control of infinite-dimensional systems using finite-dimensional techniques," Ph.D. dissertation, LIDS MIT, 1990.